TWENTY-SECOND INTERNATIONAL CONFERENCE ON COMPOSITE MATERIALS (ICCM22)

NUMERICAL MODELLING OF UHMWPE COMPOSITES UNDER IMPACT LOADING

Behjat T. Ansari[1], Mark K. Hazzard[2], Luiz F. Kawashita[1], Ulrich Heisserer[2] and Stephen R. Hallett[1]

[1] Advanced Composites Centre for Innovation and Science, University of Bristol, Bristol, UK

[2] DSM Dyneema, Geleen, The Netherlands

Keywords: Finite element analysis, Cohesive zone method, UHMWPE, Ballistic impact

ABSTRACT

The modelling of ultra-high molecular weight polyethylene (UHMWPE) fibre composites under impact loads has been the subject of numerous studies and has been attempted via different approaches. In this work, a finite element model is developed to predict the energy absorption at the interfaces of these laminates, under varying rates of impact. Cohesive elements are employed to model the behaviour of interface regions between sub-laminates at low strain rates. The model is then extended to ballistic impact rates, to capture the energy absorption mechanisms of the material and thereby facilitate better understanding of its mode I and mode II deformations. Subsequently, parametric studies are performed to determine the effect of physical parameters such as in-plane and through-thickness dimensions of the target on the dissipation of energy at the interfaces. The findings reinforce the dominance of energy dissipation through mode II delamination, while demonstrating dependence on the impact velocity.

1 INTRODUCTION

Ultra-high molecular weight polyethylene (UHMWPE) fibre composites, such as composites with Dyneema®, have caused a revolution in the field of ballistic impact protection. Developed as laminate structures, the composites are manufactured through the consolidation of ply-precursors. These plies comprise approximately 80% volume fraction Dyneema® fibres that are typically coated with resin [1,2]. Superior fibre properties, namely high tensile strength, modulus and strain to failure are traditionally credited for providing this exceptional impact performance. However, more recent studies have shed light on the role of the matrix in the behaviour of the composite laminates under impact loading. Karthikeyan *et al.* [3] highlighted the inverse relationship that exists between the matrix shear strength and the ballistic performance of composite plates, including carbon fibre reinforced plastic (CFRP) and UHMWPE composites, furthering the work of Walsh *et al.* [4], which demonstrated the necessity of the matrix medium. Low interlaminar shear strength (ILSS) has been identified as another contributor to increased energy absorption under impact loads, through altering and controlling the failure mechanism. The ILSS is typically dominated by matrix shear properties, although it has been shown to be dependent on processing parameters, such as processing pressure and temperature, to induce partial melting of the matrix during consolidation [5].

Modelling and prediction of the material behaviour under impact loading has been the subject of numerous studies and has been attempted via different approaches. While some have focused on the mechanisms through which the material deforms when subject to a single point of impact, others have placed greater emphasis on the ability to predict the impact performance of the material, as defined by either the back-face deformation (BFD) or by the ballistic limit V_{50}. Numerical models can be used as a tool for analysing the material behaviour under a wide range of impact scenarios. They can be used for predicting new impact scenarios, as well as driving design. Previous studies have investigated this behaviour through the development of multi-scale models, from beam bending [6], to hydrocodes [7].

More recently, Hazzard *et al.* [8] proposed a homogenised sub-laminate approach in the explicit finite element code LS-Dyna (Fig. 1), to model laminates of Dyneema® over a range of impact rates. Homogenisation of multiple plies at the macro-scale was deemed crucial for keeping the simulations

computationally viable, due to the low ply thickness of approximately 67.5 μm for each unidirectional (UD) layer and relatively large panel thicknesses.

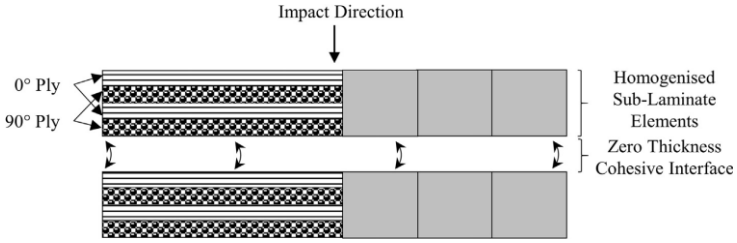

Figure 1: The sub-laminate cross-ply homogenisation approach adopted by Hazzard *et al.* [8].

2 FINITE ELEMENT ANALYSIS

In this work, the ballistic impact on a panel of Dyneema® is simulated and numerically analysed. See work by Hazzard *et al.* [8] for threat and target material models, along with experimental validation using publicly available data from literature [9].

2.1 Interface modelling

Generally, delamination is perceived to be one of the most critical modes of failure in laminated composites, as a result of their relatively poor through-thickness and interfacial performance [10]. Under high rates of impact however, UHMWPE composites can readily deform and delaminate in the normal direction and particularly in the shear direction. The extent of deformation via these mechanisms is a determining factor of the level of energy absorbed under impact, and hence the impact performance [3]. Since the delamination fracture process is generally dominated by matrix properties and is of a mixed-mode nature, it is imperative to consider the deformation of the composite material in both mode I and mode II. Likewise, their combined effect must be considered due to the influence of mode-mixity. Thus, the purpose of this study is to develop a better understanding of the composite deformation mechanisms by approaching the inter-laminar interface modelling with an element-based (E-B) cohesive zone method (CZM).

2.2 Cohesive zone method

Cohesive zone models are considered most suitable for modelling interlaminar failure of composite laminates, since the energy required for crack propagation can be accounted for, which is a limitation of a stress-based approach [7]. This approach assumes that the contribution of delamination to the total amount of energy absorbed is relatively small. According to Peijs *et al.* [11] however, in high-performance polyethylene/epoxy composites (Spectra™/Araldite™ LY556/HY917/DY070) energy absorption through this failure mode accounts for a tenth of the total impact energy with the rest contributed to energy absorption by fibre fracture, beneficial for low velocity impacts.

The current study is based on the work of Hazzard *et al.* [8], where MAT162 by Materials Science Corporation was selected for representing homogenised cross-ply sub-laminates of Dyneema® HB26, due to its sophistication in modelling composite damage and failure [12]. MAT162 is a rate-dependent progressive damage model for composites, with the ability to incorporate parameters such as cross-ply damage criteria, as well as capturing additional failure modes, non-linear damage and strain rate effects, deeming it the most suitable for modelling the behaviour of this material. Hazzard *et al.* [8] modelled the contact behaviour between homogenised sub-laminates using cohesive surface-to-surface contact in LS-DYNA, employing the tiebreak contact option with the DYCOSS algorithm [13] to provide a mixed-mode bilinear traction separation law to capture the delamination of the composite. In order to accurately capture the low shear strength of the matrix and interface, and the resulting limited transfer of load between the sub-laminates, the authors proposed that the traction stiffness values of the interface should be scaled inversely to the sub-laminate thickness, for the reason that the thickness of each layer implicitly represents the number of interfaces that are present in the homogenised stack. As a result of homogenisation of individual plies in this method, it is vital to capture the contribution of the interface between each sub-laminate, and therefore the role that the matrix properties play in

this. The larger the sub-laminate thickness, the higher the number of interfaces at which the layers can deform. The mode I traction stiffness, K_I, is calculated as

$$K_I = E_m/h_{SL}, \quad (1)$$

where h_{SL} is the sub-laminate thickness and E_m is the Young's modulus of the matrix, while the mode II equivalent, K_{II}, is approximated as 60% of K_I. Although this model yields realistic indications of the energy absorbed by the interface through mode I and mode II deformations under impact, the values obtained are of a mixed-mode nature. It would be valuable to isolate the two modes of deformation in order to investigate the effect of the different interface fracture parameters, determined by the matrix properties, on the impact performance of the material. One such approach utilises E-B cohesive models [14] to describe the interface between the homogenised sub-laminate layers of a fibre-reinforced composite structure. With the implementation of the Bristol Cohesive UMAT [15], strain energy release rate of the elements in the two modes of fracture can be extracted and attributed to the total energy released at the interface.

2.3 Cohesive element implementation

Cohesive elements were implemented at the interfaces of sub-laminates, sharing nodes with elements in the layers above and below, as demonstrated in Fig. 2 (b). Under quasi-static rates representing drop weight impact (DWI) tests performed at 3.37 m/s, the E-B cohesive zone approach yields comparable force-displacement results to the tiebreak contact with the surface-based (S-B) cohesive formulation (Fig. 2 (a)). The introduction of the cohesive elements with zero volume resulted in the reduction of simulation timestep, thereby increasing the computation time significantly. This was counteracted by taking advantage of the symmetric loading and geometry to reduce the model size to a quarter, while scaling the results by a factor of four (Fig. 2 (a)). Since low impact velocity does not lead to failure, no additional contact definition was required between the laminate layers.

Under ballistic impact, failure of cohesive elements leads to their erosion. An additional form of contact was therefore required to maintain the contact definition between the layers throughout the simulation. A single surface eroding contact with *SOFT* option equal to 2 was found most suitable for this purpose. It must be noted that there is also a requirement for additional contact in the tiebreak contact case. The purpose of this is to prevent inter-part penetration of sub-laminates and subsequent negative contact energy values, similar to the purpose of gaps between sub-laminate layers in models incorporating bonded contact with stress-based failure criteria [7]. Following the implementation of the two forms of contact definition, projectile through-thickness velocity v and V_{50} predictions were plotted in Fig. 3 (a) and Fig. 3 (b), where they look reasonably well-aligned.

3 INTERFACE ENERGY DISSIPATION

The overall contribution of the interface to the dissipation of the kinetic energy of a 55 g steel FSP was investigated for a panel with 300 x 300 mm in-plane dimensions, 10 mm thickness and 1 mm sub-laminate thickness, using element-based cohesive interface layers. This was performed for two cases, a stop case at an impact velocity of 350 m/s, and the other a perforation case at 600 m/s. In addition, the contribution of each individual interface was investigated to demonstrate the variation of this based on proximity to the projectile in the through-thickness direction. In order to quantify and visualise the extent of energy dissipation, mode I and mode II strain energy release rates were extracted from the model for every element at each interface. The values extracted are element averages that are based on the values at the four Gauss integration points of the *ELFORM* = 19 solid elements. These points exist on the element mid-surface, the mid-point between the top and bottom surfaces of the solid elements [13]. The energy dissipated at each element, E_{el}, at time t was calculated as the product of the energy release rate at that element at that point in time, G_{el}, and the initial surface area of the zero-thickness cohesive element mid-surface, A_{el}. It was assumed that the variation in the in-plane dimensions of the interface elements over time are negligible for the purpose of these calculations, allowing the element area at $t = 0$ to suffice for the entire impact duration. The energy dissipated at the interface, I_nE, can be represented by the sum of the energy dissipated by all the elements at that interface over time, where n is the interface number, with $n = 1$ representing the interface next to the strike face and thus in closest

proximity to the projectile, using

$$I_nE(t) = \sum_{n_{el}=1}^{n_{el}} G_{el}(t) \cdot A_{el}(t_0), \tag{2}$$

It is worth noting that energy values over time are given as cumulative sums. For example, the value of I_nE at time t is equal to

$$\sum_{t=0}^{t} I_nE(t). \tag{3}$$

3.1 Global energy dissipation

To distinguish between different modes of fracture, the term for general energy dissipation at a single interface, I_nE, can also be represented by I_nE_I and I_nE_{II}. These refer to the energy dissipated at interface n through mode I and mode II fracture, respectively, while mixed-mode fracture energy equal to the sum of I_nE_I and I_nE_{II} can be denoted by I_nE_T. The sum of the energy dissipated at all interfaces in the entire material system at time t is given by I_TE(t). The kinetic energy of projectile KE_p(t), determines the total amount of energy that is dissipated by the entire laminate, $TE(t)$, such that

$$TE(t) = KE_p(t_0) - KE_p(t). \tag{4}$$

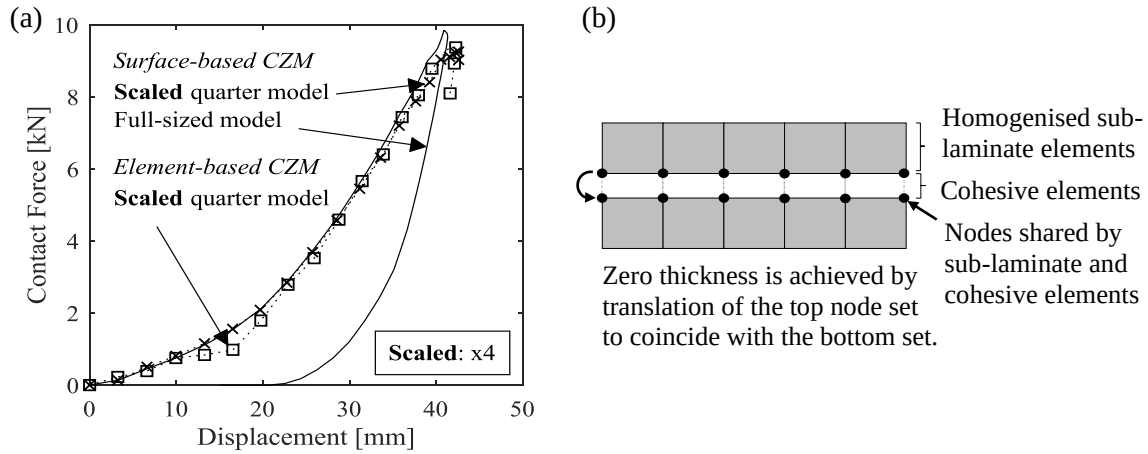

Figure 2: (a) Comparison of contact force against displacement between S-B and E-B CZM for DWI tests, (b) implementation of cohesive elements at the interfaces between sub-laminates.

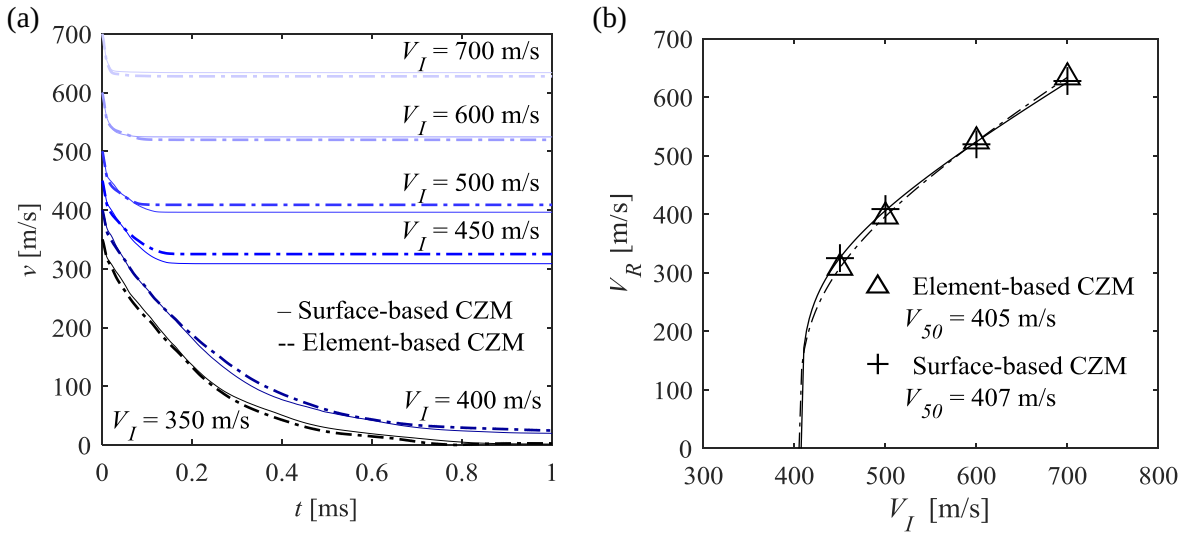

Figure 3: Comparison between S-B and E-B CZM for ballistic impact, in terms of (a) projectile velocity and (b) Lambert-Jonas curve fits.

The I_TE(t) term is normalised with TE(t), and therefore indirectly with the kinetic energy of the projectile, to demonstrate how much of the total energy dissipation takes place at the interfaces. In Fig. 4, I_TE and I_TE/TE are plotted over the duration of impact, comparing a stop case at V_I = 350 m/s to a perforation case at V_I = 600 m/s. There is an equivalent rate of dissipation in both cases until 0.1 ms (Fig. 4 (a)), by which point the projectile has either slowed down, relative to the target, to a velocity that inflicts no further substantial damage to the sub-laminates, or has fully perforated the laminate, as shown by the corresponding snapshots of the laminate cross-sections in Fig. 5. The first 0.1 ms are critical as they determine whether the laminate is perforated. If fully perforated, the implications of the laminate behaviour will no longer be as relevant. When the projectile is stopped however, the BFD becomes the key indicator of impact performance for the remainder of the impact duration. In both cases, the interface continues to dissipate energy after t = 0.1 ms, albeit at a lower rate. Membrane bulging is known to contribute to higher levels of energy dissipation than the more localised damage which occurs in the progressive failure regime in the earlier stages of impact [16]. The absolute amount of energy dissipated through in-plane modes continues to rise linearly until the end of the simulation at t = 1 ms. Naturally, if the laminate is fully perforated, the rate of dissipation is substantially reduced after t = 0.1 ms, whereas in the stop case, the laminate continues to dissipate the kinetic energy of the projectile that it is in contact with, at a similar rate to the earlier stages of impact.

From t = 0.1 onwards, the contribution of mode II deformations to the total mixed-mode dissipation (Fig. 4 (b)) falls by 3% (V_I = 350 m/s) and by 4% (V_I = 600 m/s) from t = 0.1 ms to t = 0.2 ms, while the contribution of mode I dissipation grows. Following perforation, while mode II shearing still accounts for most of the energy dissipation, it is the rise in the out-of-plane delamination that is most noticeable in the perforation case, the extent of which exceeds the mode I dissipation of the stop case. This can be attributed to continued delamination of the sub-laminate layers close to the strike face, as seen in Fig. 5 (b), after the projectile has passed through, in addition to the inclusion of the elements that have been disconnected from the laminate during perforation. These elements continue to travel together with the projectile until each layer is propelled off course into a different direction, visible in the inserts in Fig. 5 (b). This is verified in the following section, by considering the contribution of each interface separately. Similarly, the increase in mode I energy dissipation is demonstrated by the increased delamination of the perforated sub-laminates and the progression of the shear hinge on the back face in Fig. 5 (a). The mode II and therefore the mixed-mode rates of dissipation approach zero, with the curves plateauing over time as a result of the impactor coming to a complete halt and no longer having any kinetic energy to be dissipated by the laminate. Although the absolute amount of energy absorbed by the stop case is substantially higher after t = 0.1 ms, the difference between the two cases is minimal when the values are compared as a proportion of the total energy absorbed by the laminates in Fig. 4 (b). In addition, energy dissipated at the laminate interfaces is seen to continuously rise over the course of impact as a portion of the total energy dissipated by the entire laminate. Following perforation, no more energy can be transferred from the projectile to the laminate. However, in the laminate energy can be redistributed from momentum transfer and internal energy (Fig. 6 (b)) through the interface, which continues to absorb energy during this transfer.

The flat region of V_I = 350 m/s *Total* and *Mode II* curves in Fig. 4 (b) represents the period during which the projectile is slowed down the most (Fig. 3 (a)) and ceases penetration of further layers. The sub-laminate layer at which this occurs is under significant strain, as visualised by the cross-section of the model at t = 0.15 ms in Fig. 4 (b). The larger the extent of stretching, the greater the amount of energy that is absorbed through internal energy of the fibres, as demonstrated by the rise in internal energy of sub-laminates in Fig. 6 (a) and the contribution of this to the total amount of energy dissipated by the laminate (Fig. 6 (b)). Each sub-laminate is identified by m, with m = 1 representing the layer on the front face of the target. While the largest percentage of internal energy absorption occurs at the point of contact, particularly in the sub-laminate layers directly under the path of the projectile (Fig. 6 (c)), there is also a rise to almost 4% in the unperforated layers between t = 0.1 ms and t = 0.3 ms, coinciding with the relatively flat region of the aforementioned curves in Fig. 4 (b).

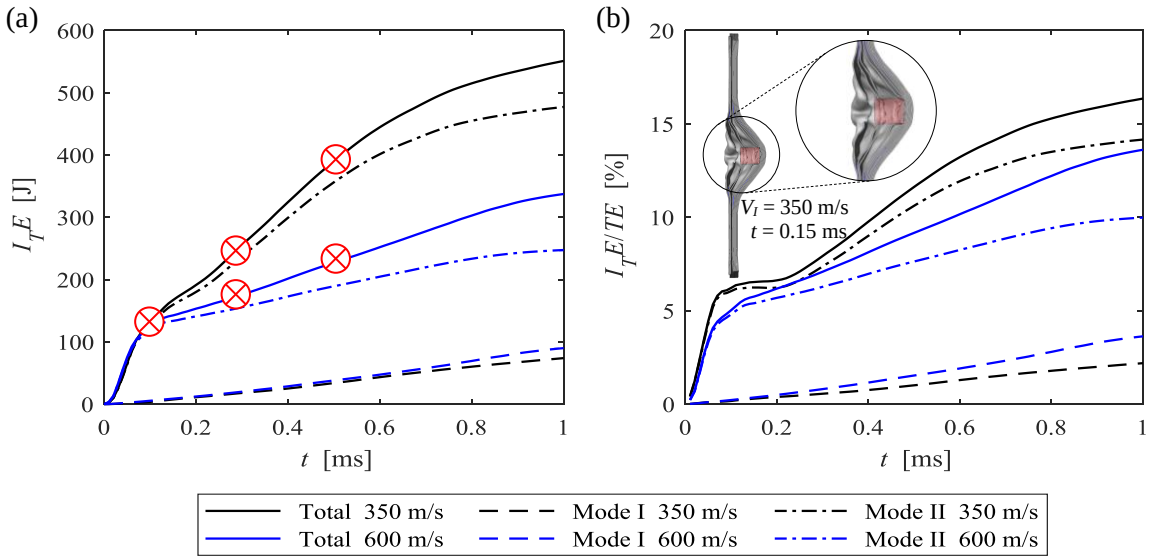

Figure 4: (a) Energy dissipated at interfaces during impact at V_I = 350 m/s and V_I = 600 m/s, (b) energy dissipated at interfaces as a percentage of total energy dissipated.

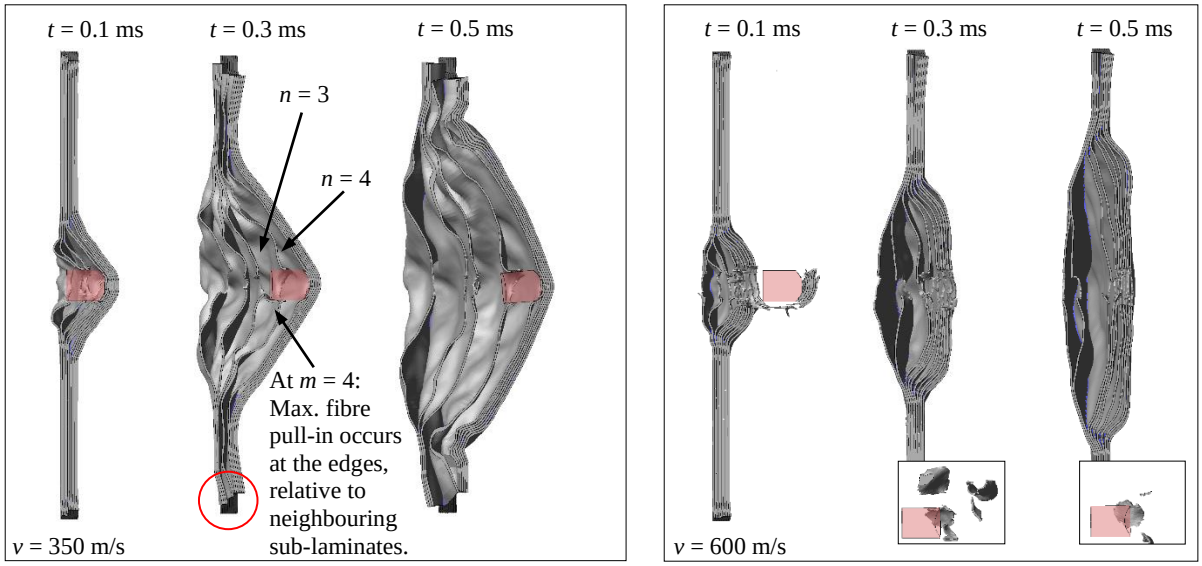

Figure 5: Progression of projectile and deformation of laminate at discreet points in time after impact.

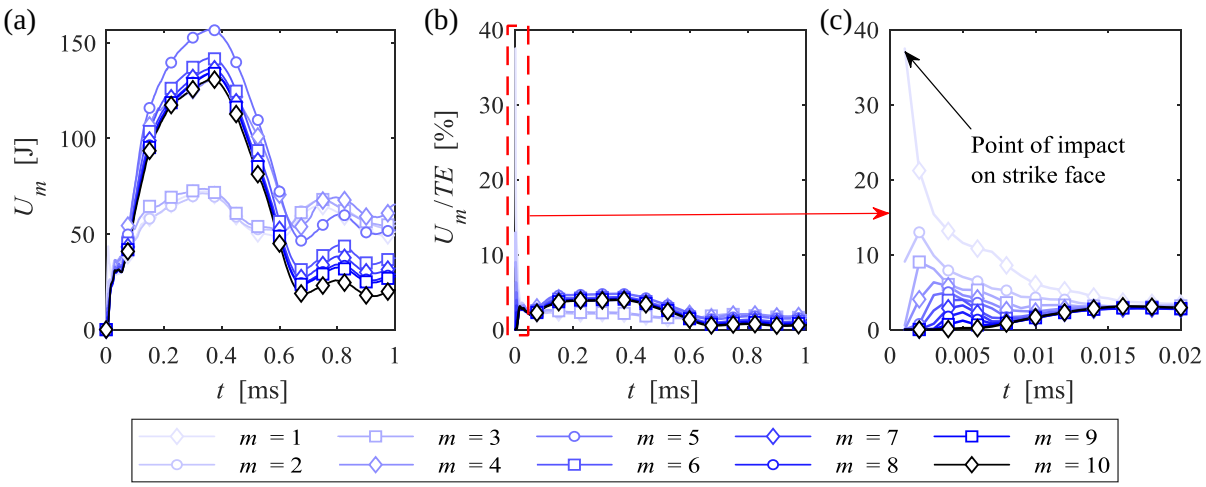

Figure 6: Internal energy of sub-laminate layers under impact at V_I = 350 m/s, in terms of (a) absolute values per layer, (b) and (c) contribution of each layer to total energy absorbed.

3.2 Local energy dissipation

The contribution of each interface to the total energy dissipated at the interfaces is visualised in Figs. 7 and 8 for the semi- and full-perforation cases, respectively. The lighter the colour of the curve, the closer the proximity of the interface it represents to the strike face. The subplots demonstrate the energy absorbed through mode I, mode II and mixed-mode deformations. As per the overall interface results, the local mixed-mode behaviour at the sub-laminate level is dominated by mode II deformation for all layers in both instances. Descriptions of the mode II behaviour will therefore also reflect the overall deformation of each layer. In Fig. 7 (a), mode I energy dissipation is consistent across all interfaces, until further damage is prevented prior to t = 0.2 ms. From this point onwards, there is substantial reduction in the rate of mode I dissipation at the third interface. Figure 5 (a) demonstrates the projectile getting stopped after having fully perforated the first three sub-laminate layers. From the fourth sub-laminate layer onwards, the laminate undergoes extensive amounts of in-plane shear, as a result of pull-in of primary fibres from the edges. The effects are captured by the corresponding interfaces above and below the fourth sub-laminate layer (n = 3 and n = 4), portraying the large mode II deformations experienced by these elements relative to elements in the neighbouring sub-laminates. This is most visible at the edges of the plate, highlighted at t = 0.3 in Fig. 5 (a).

Beyond n = 3, slightly higher levels of energy are absorbed at the interface following transition to the membrane/bulge mode, which is in line with previous observations reporting on the prevalence of membrane deformation, particularly interlaminar shear in laminates thinner than 20 mm, impacted at velocities below 600 m/s [1,16]. At n = 3, around twice as much energy is dissipated in mode II than at the other interfaces, shown in Fig. 7 (b), throughout the length of the simulation. One exception is the fourth interface, at which the laminate switches from a local failure regime, to a membrane bulging phase. At n = 4, mode II energy dissipation increases rapidly until reaching 33 J, after which point the FSP is caught by the laminate and therefore restricts membrane motion in the surrounding interface. This leads to the following reduction in the rate of mode II energy dissipation at the fourth interface (Fig. 7 (b)). While energy continues to be dissipated at all interfaces, the layers below the projectile continue to do so at a constant rate until after t = 0.6 ms. By contrast, the layers above the projectile move towards total delamination and separation, due to the complete failure of these interface layers and tear off from the rear face of the laminate. This limits further potential dissipation at these locations, thereby slowing the rate of energy dissipation towards the end of the simulation. In the total perforation case in Fig. 8, mode I dissipation of energy (Fig. 8 (a)) is seen to play an increasingly larger role in the overall energy dissipation (Fig. 8 (c)) at the interfaces compared to the lower impact velocity, while the contribution of the interfaces in mode I dissipation remains relatively consistent, with I_nE_I ranging from 0.4 J to 0.9 J until the point of total perforation of the laminate at t = 0.10 ms. Beyond this point, there is an increase in the rate of dissipation at the interfaces closest to the back face. It was found that the further progression of the shear hinge towards the back face of the panel results in a larger area of the interface dissipating energy in mode I. The closer the layers are to the rear face, the larger the area covered by the shear hinge and therefore the larger the mode I energy at the interfaces between them, as a result of the redistribution of energy dissipated by the laminate. At t = 0.5, failure occurs in a significant proportion of the two interfaces closest to the back face at n = 8 and n = 9, hence giving rise to the drop in the rate of dissipation visible in Fig. 8 (a).

Figure 8 (b) displays the corresponding mode II dissipation at each layer for V_I = 600 m/s. Upon impact, there is an immediate rise in the energy dissipated at all interfaces, including those not in contact with the projectile. The progressive nature of failure in the first three sub-laminates is visible in the mode II energy dissipation at their neighbouring interfaces (n = 1 to n = 3). In a similar manner, at around 10 J, the final two interfaces (n = 8 and n = 9) contribute to around half as much mode II energy dissipation as the middle interfaces at the point of full perforation. The sub-laminates towards the rear face of the panel have failed through fibre tensile failure [1,17], following the arrival of the transverse pressure wave at the back face and the subsequent pull-in action under the path of the projectile, thus leaving less potential for energy absorption through delamination. Interfaces n = 4 to n = 7 are therefore responsible for the bulk of mode II interface energy dissipation. These interfaces are

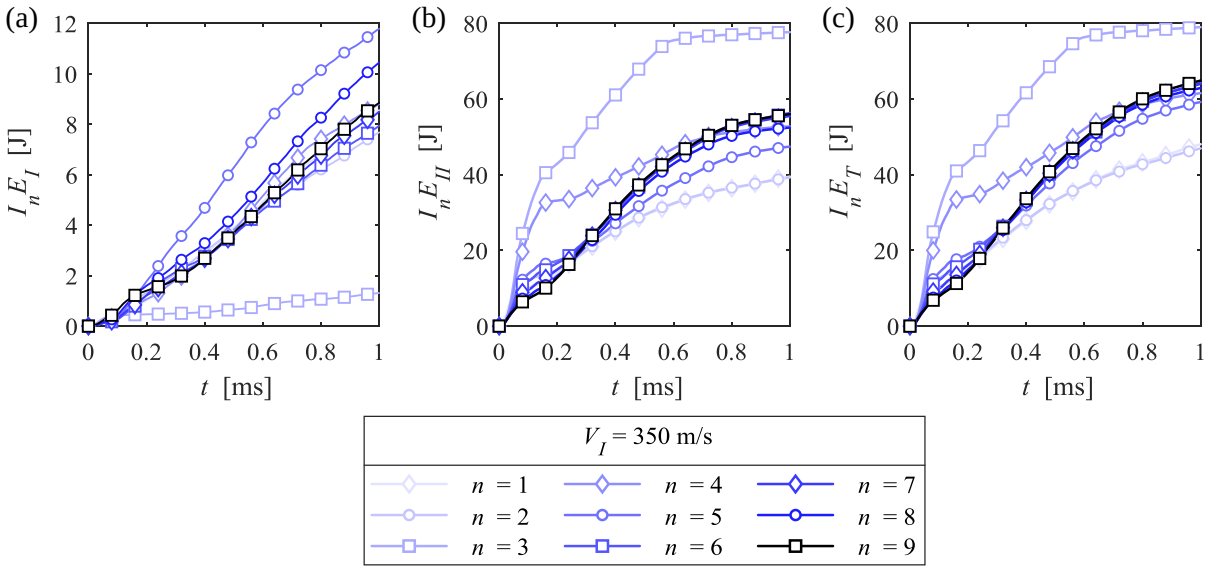

Figure 7: Energy dissipated at each sub-laminate layer under impact at V_I = 350 m/s, through (a) mode I, (b) mode II (c) and mixed-mode delamination.

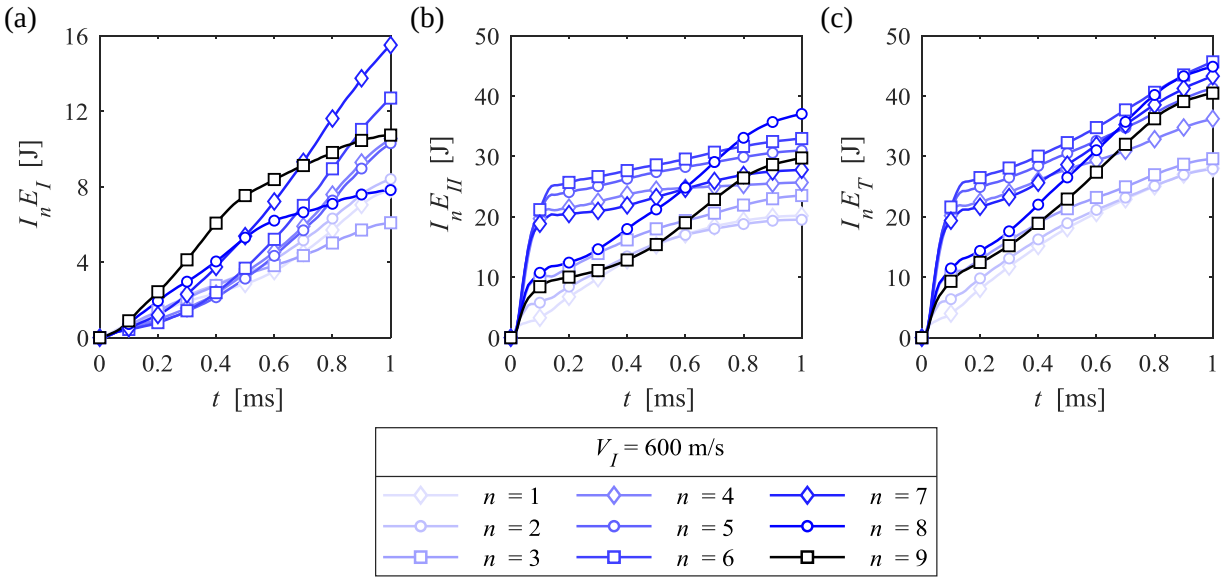

Figure 8: Energy dissipated at each sub-laminate layer under impact at V_I = 600 m/s, through (a) mode I, (b) mode II (c) and mixed-mode delamination.

adjacent to the sub-laminates with the largest shear pull-in of primary fibres. Upon perforation, the rate of dissipation is radically reduced at the interface below the relevant sub-laminate. Following perforation, all interfaces continue to dissipate energy in mode II due to energy exchange within the laminate. The rate at which this occurs depends on the extent of energy dissipated prior to perforation; the smaller and more localised the failure, the larger the rate of dissipation following perforation.

4 PARAMETRIC STUDIES

4.1 Impact velocity

Figure 9 demonstrates the consistency in the rate of dissipation of energy through delamination across a range of strike velocities up to a point of transition in the penetration mode, or total perforation. This occurs almost entirely in mode II, followed by a gradual increase in the contribution of mode I dissipation. The similarity in the rate of dissipation arises from the local failure regime, the extent of which increases with V_I. In the range of velocities considered, the amount of energy dissipated is highly sensitive to V_I, with an increase of 50 m/s leading to a rise of 50 J in I_TE.

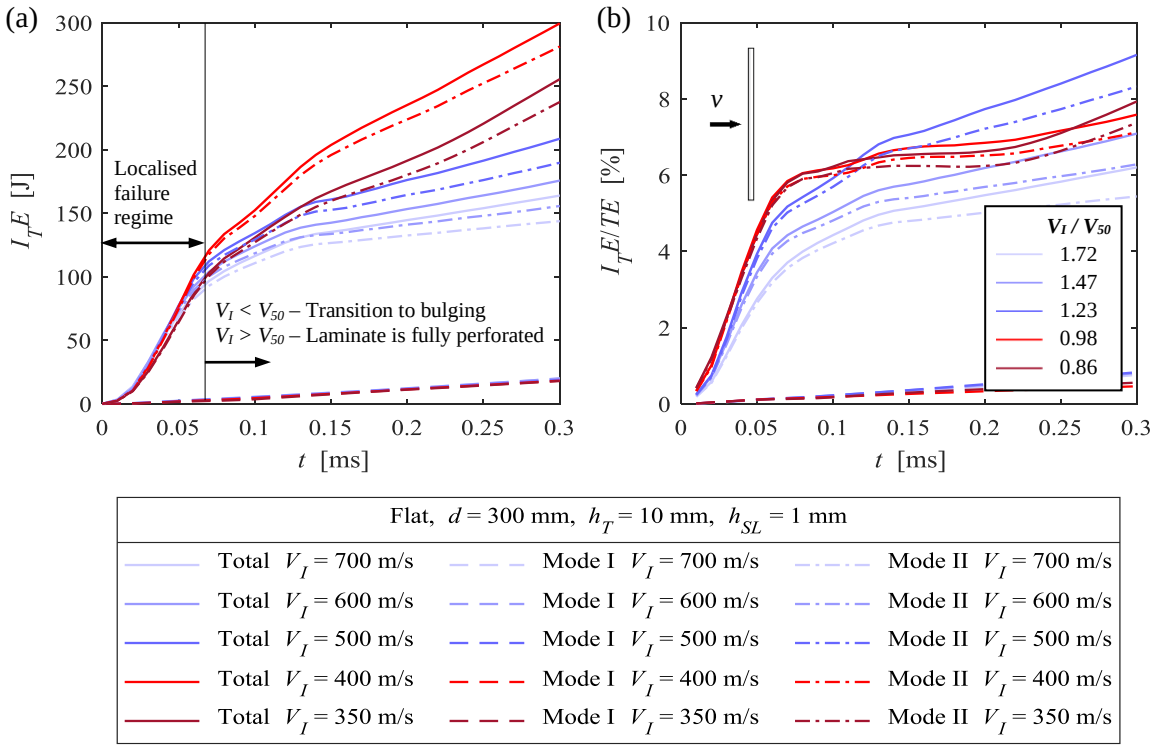

Figure 9: (a) Energy dissipated at interfaces and (b) energy dissipated at interfaces as a percentage of total energy dissipated by laminate, for a range of impact velocities.

It is worth noting that total energy is highest at velocities closest to the V_{50}. Meanwhile, impact velocities exceeding the V_{50} result in full perforation, together with the rate of energy absorption falling with increasing values of V_I. According to Fig. 9 (b), however, the trends in $I_T E$ /TE are almost identical for $V_I < V_{50}$, while clear distinctions can be made when $V_I > V_{50}$, even prior to perforation.

4.2 In-plane and out-of-plane dimensions

In Fig. 10, dimension d represents the length of the square target. Targets with smaller in-plane dimensions tend to have higher ballistic limits due to the smaller distance from the centre of the target to the edges, which facilitates easier pull-in of primary fibres in the sub-laminate. As previously reported in literature [8,18], plates with d < 300 mm in simulations without boundary conditions holding the targets in place end up accelerating with the projectile rather than being subjected to penetration, due to insufficient momentum to hold them in place. These simulations could be repeated with a support plate that prevents this motion from occurring. The increase in the energy absorbed with d is expected, due to the expansion in the interface area where energy can be dissipated. At both impact velocities used here, the differences in $I_T E$ /TE become minimal when $d \geq$ 300 mm, since the plate is no longer set in motion by the projectile. This effect is much more pronounced in the higher velocity case (Fig. 10 (b)), where a smaller extent of the total energy is dissipated at the interfaces due to the absence of the binary bulging mechanism that follows the progressive regime when V_I = 350 m/s.

The effect of the total laminate thickness h_T on $I_T E$ /TE is displayed in Fig. 11. The trends reflect what has previously been reported in literature regarding the effect of laminate thickness on impact performance [19,20]. Once again, this disparity in behaviour arises from differences in the penetration mechanisms that take place. Since these mechanisms [4,17] and therefore the depth of penetration [21] are determined by V_I and V_{50}, the ratio between the two are given for each plate thickness in Figs. 11 (a) and (b). In both cases, the impact velocity exceeds the ballistic limit of the thinnest plate (h_T = 5 mm), while not reaching the ballistic limit of the thickest target (h_T = 20 mm). However, the influence of the ballistic limit on the rate of energy absorption of the laminate does not explain the large differences that exit between plates with 8 mm $\leq h_T \leq$ 15 mm, and those with the minimum and maximum thickness values, under both impact velocities. Likewise, questions remain regarding the exact thickness values below and beyond which the interfaces see a drastic rise or fall in terms of their contribution to the overall energy dissipation, warranting further investigation into this matter.

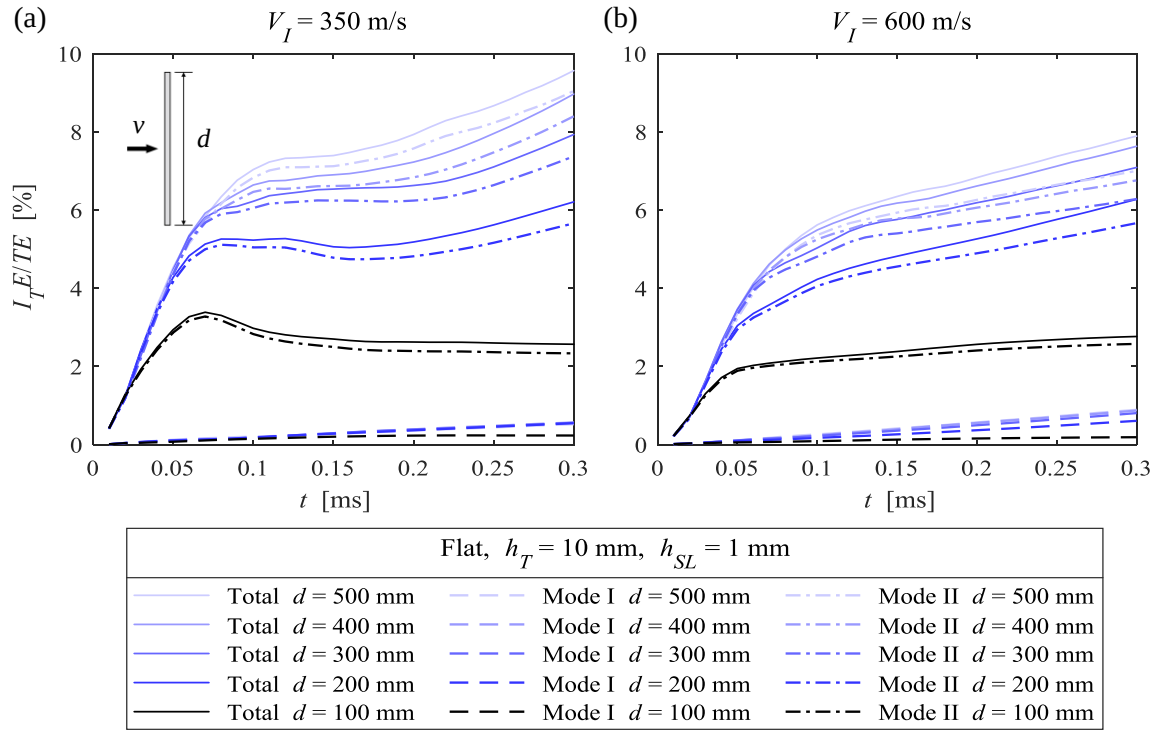

Figure 10: Energy dissipated at interfaces as a percentage of total energy dissipated by laminate for a range of in-plane plate dimensions at (a) V_I = 350 m/s, and (b) V_I = 600 m/s.

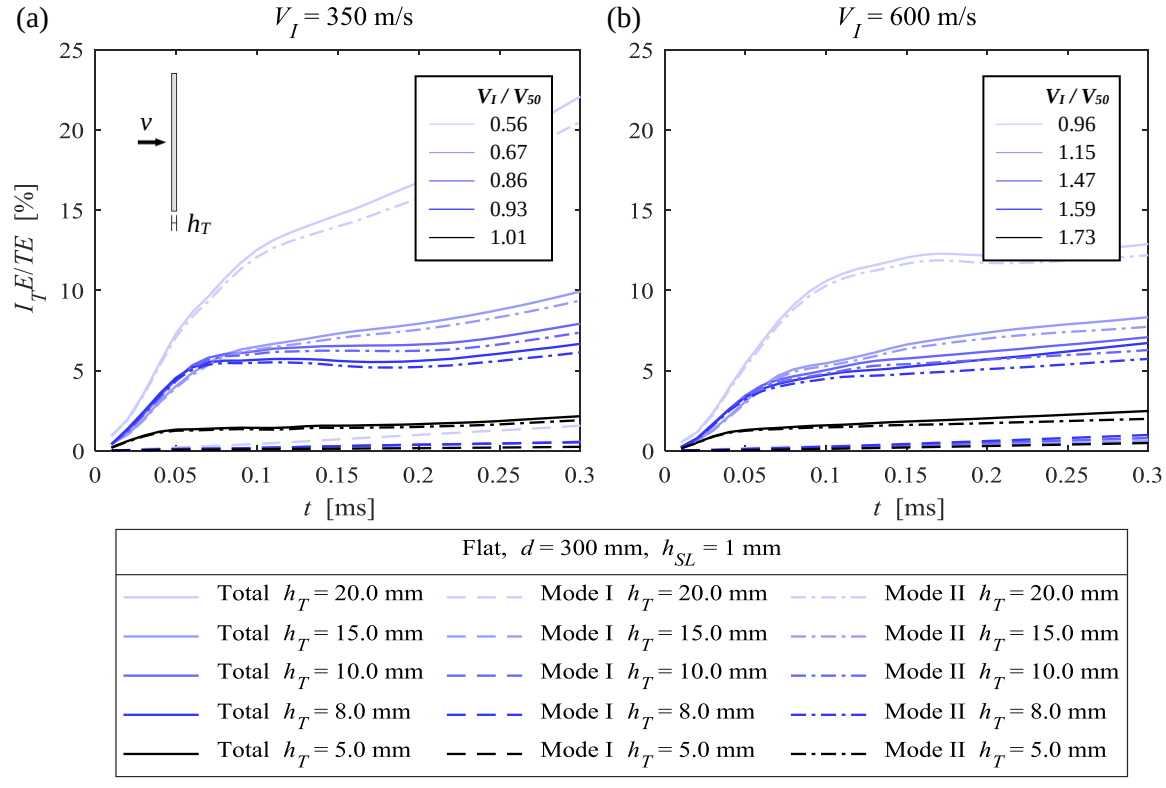

Figure 11: Energy dissipated at interfaces as a percentage of total energy dissipated by laminate for a range of plate thicknesses at (a) V_I = 350 m/s, and (b) V_I = 600 m/s.

At the lower end of the thickness spectrum, these differences have previously been attributed to the sole action of the binary failure regime in laminates with low areal densities [16], compared to the multi-stage failure regimes of higher areal density laminates. In the case of thicker laminates however,

ductile tensile failure has previously been observed at the back face of targets, believed to have been a result of shock induced temperature increase [17]. Thus, the applicability of the current model could be limited for laminate thicknesses above 15 mm, due to the negligence of temperature effects. Furthermore, capturing local failure mechanisms such as indirect tension becomes increasingly important with thicker laminates, as a larger portion of the laminate fails in this manner due to the different Poisson expansion between the 0° an 90° cross-ply layers in the through-thickness direction [20,22]. It is also worth noting that the homogenisation approach does not account for ply thickness, which is known to affect performance.

5 CONCLUSIONS

Regarding energy dissipation at the interface, this study has identified the following:

- Energy is dissipated at the same rate in partial- and full- perforation cases, until the deformation mode switches from localised failure to distal membrane bulging or until full perforation.
- After this point, the laminates in both cases continue to dissipate energy at the interfaces, although at a much higher rate in the laminate that was not fully perforated, since the un-perforated layers continue to deform through in-plane shear via bulging.
- In terms of contribution to overall energy absorption, the two cases yield comparable results, both dominated by mode II deformation.
- The role of the interface grows over time, until the kinetic energy of the projectile is fully absorbed, or the interfaces have failed completely, causing the sub-laminates to become completely detached. This is particularly significant when $V_I < V_{50}$, as the ability of the laminate to dissipate energy following the arrival of the transverse relief wave at the front of face of the projectile will determine the extent of trauma caused to the wearer in body armour applications.
- At V_I = 600 m/s, the contribution of mode I energy dissipation to the mixed-mode total higher than at the lower velocity, suggesting that mode-mixity is influenced by V_I.

The contribution of individual interfaces was examined, and the following observations were made:

- In both fracture modes, V_I determines the proportion of energy dissipated through delamination at each interface relative to the other interfaces.
- Naturally, the behaviour of the interfaces mimics the deformation of neighbouring sub-laminate elements, thus leading to a dependency of energy dissipation at individual interfaces on V_I.
- For $V_I < V_{50}$, the interface at which the penetration mode transitions from local failure to membrane bulging accounts for four times as much mode II energy dissipation than almost all the other interfaces at the point when the mode switches, closely followed by the interface directly below the sub-laminate layer that is not perforated.
- The same interface accounts for the smallest contribution to mode I dissipation, likely due to extensive delamination in mode II at the periphery of the projectile body.
- For $V_I > V_{50}$, the interfaces with the largest contribution to mode II energy dissipation are the middle interfaces, where interaction with the shockwave occurs.

Parametric studies have revealed that:

- Below the V_{50}, I_TE increases with V_I, with larger increases as V_I approaches the V_{50}. The trend reverses beyond the V_{50}, with the reduction in the energy levels converging at higher values of V_I, reflecting the shift in failure modes and rate of energy dissipation of the laminate as a whole.
- The contribution of the interface as a percentage of total energy dissipation is relatively insensitive to V_I below the ballistic limit, while becoming more relevant at $V_I > V_{50}$.
- Targets with larger in-plane dimensions demonstrated higher levels of I_TE /TE, as a result of the increased interface area. The increase was, however, not very significant for both partial and total perforation, since larger plate dimensions lead to more energy being absorbed via other means.
- Overall, I_TE /TE is not seen to be as sensitive to laminate thickness as it is to other parameters, regardless of the impact velocity for the two V_I cases that were explored, unless considering extreme changes such as doubling or halving of the baseline laminate thickness of 10 mm. The

extensive differences in the extreme cases are partially down to modelling deficiencies, while also highlighting the differences in the failure mechanisms of laminates of varying thickness.

To summarise, the contribution of energy absorbed through delamination in a laminate with Dyneema® can be predicted with an element-based cohesive approach in finite element analyses. Further investigations will be carried out to determine the accuracy of this regarding the capturing energy dissipation through delamination. Subsequent work will include investigation of the in-plane distribution of energy dissipation, as well as steps to improve the numerical model to include rate-effects at the interface, as the matrix is inherently rate and pressure sensitive. The results of this would then be of significance for component design.

6 ACKNOWLEDGEMENTS

The authors would like to acknowledge the Engineering and Physical Sciences Research Council for their support through the Centre for Doctoral Training in Advanced Composites for Innovation and Science at the Bristol Composites Institute (ACCIS), and DSM Dyneema® for their continued support and funding of this research. Dyneema® is a trademark of Royal DSM NV.

7 REFERENCES

[1] B. P. Russell, K. Karthikeyan, V. S. Deshpande, and N. A. Fleck, "The high strain rate response of ultra high molecular-weight polyethylene: from fibre to laminate," *Int. J. Impact Eng.*, vol. 60, pp. 1–9, 2013.

[2] H. Van Der Werff and U. Heisserer, "High-performance ballistic fibers: Ultra-high molecular weight polyethylene (UHMWPE)," in *Advanced Fibrous Composite Materials for Ballistic Protection*, 1st ed., X. Chen, Ed. Woodhead, 2016, pp. 71–108.

[3] K. Karthikeyan, B. P. Russell, N. A. Fleck, H. N. G. Wadley and V. S. Deshpande "The effect of shear strength on the ballistic response of laminated composite plates". *European Journal of Mechanics - A/Solids*, Vol. 42, pp 35-53, 2013.

[4] T. F. Walsh, B. H. Lee, and J. W. Song, "Penetration Failure of Spectra® Polyethylene Fiber-Reinforced Ballistic-Grade Composites," *Key Eng. Mater.*, vol. 141–143, pp. 367–382, 1998.

[5] E. S. Greenhalgh, V. M. Bloodworth, L. Iannucci, and D. Pope, "Fractographic observations on Dyneema® composites under ballistic impact," *Compos. Part A Appl. Sci. Manuf.*, vol. 44, pp. 51–62, 2013.

[6] G. Liu, M. D. Thouless, V. S. Deshpande, and N. A. Fleck, "Collapse of a composite beam made from ultra high molecular-weight polyethylene fibres," *J. Mech. Phys. Solids*, vol. 63, pp. 320–335, 2014.

[7] L. H. Nguyen, T. R. Lässig, S. Ryan, W. Riedel, A. P. Mouritz, and A. C. Orifici, "A methodology for hydrocode analysis of ultra-high molecular weight polyethylene composite under ballistic impact," *Compos. Part A Appl. Sci. Manuf.*, vol. 84, pp. 224–235, 2016.

[8] M. K. Hazzard, R. S. Trask, U. Heisserer, M. Van Der Kamp, and S. R. Hallett, "Finite element modelling of Dyneema® composites: From quasi-static rates to ballistic impact," *Compos. Part A Appl. Sci. Manuf.*, vol. 115, no. July, pp. 31–45, 2018.

[9] L. H. Nguyen, S. Ryan, S. J. Cimpoeru, A. P. Mouritz, and A. C. Orifici, "The effect of target thickness on the ballistic performance of ultra high molecular weight polyethylene composite," *Int. J. Impact Eng.*, vol. 75, pp. 174–183, 2015.

[10] J. K. Kim and Y. W. Mai "Engineered Interfaces in Fiber Reinforced Composites". 1st edition, Elsevier Science, 1998.

[11] T. Peijs, H. A. Rijsdijk, J. M. M. de Kok, and P. J. Lemstra, "The role of interface and fibre anisotropy in controlling the performance of polyethylene-fibre-reinforced composites," *Compos. Sci. Technol.*, vol. 52, no. 3, pp. 449–466, 1994.

[12] B. A. Gama and J. W. Gillespie, "Finite element modeling of impact, damage evolution and penetration of thick-section composites," *Int. J. Impact Eng.*, vol. 38, no. 4, pp. 181–197, 2011.

[13] J. O. Hallquist, "LS-DYNA Keyword User's Manual, vol. I," 2007.

[14] Y. Mi, M. A. Crisfield, G. A. O. Davies, and H. B. Hellweg, "Progressive delamination using interface elements," *J. Compos. Mater.*, vol. 32, no. 14, pp. 1246–1272, 1998.

[15] W. G. Jiang, S. R. Hallett, B. G. Green, and M. R. Wisnom, "A concise interface constitutive law for analysis of delamination and splitting in composite materials and its application to scaled notched tensile specimens," *Int. J. Numer. Methods Eng.*, 2007.K. Karthikeyan and B. P. Russell, "Polyethylene ballistic laminates: Failure mechanics and interface effect," *Mater. Des.*, vol. 63, pp. 115–125, 2014.

[16] K. Karthikeyan, B. P. Russell, N. A. Fleck, M. O'Masta, H. N. G. Wadley, and V. S. Deshpande, "The soft impact response of composite laminate beams," *Int. J. Impact Eng.*, 2013.

[17] C. Grunwald, T. Lässig, H. van der Werff, U. Heisserer, L. Nguyen, and W. Riedel, "Numerical sensitivity study of ballistic impact on UHMWPE composites," in *6th International Conference on Design and Analysis of Protective Structures, DAPS 2017*, 2017.

[18] B. L. Lee, J. W. Song, and J. E. Ward, "Failure of Spectra® Polyethylene Fiber-Reinforced Composites under Ballistic Impact Loading," *J. Compos. Mater.*, vol. 28, no. 13, pp. 1202–1226, 1994.

[19] M. R. O'Masta, B. G. Compton, E. A. Gamble, F. W. Zok, V. S. Deshpande, and H. N. G. Wadley, "Ballistic impact response of an UHMWPE fiber reinforced laminate encasing of an aluminum-alumina hybrid panel," *Int. J. Impact Eng.*, vol. 86, pp. 131–144, 2015.

[20] U. Heisserer, H. Van Der Werff, and J. Hendrix, "Ballistic depth of penetration studies in Dyneema® composites," in *Proceedings - 27th International Symposium on Ballistics, BALLISTICS 2013*, 2013, vol. 2, pp. 1936–1943.

[21] J. P. Attwood, B. P. Russell, H. N. G. Wadley, and V. S. Deshpande, "Mechanisms of the penetration of ultra-high molecular weight polyethylene composite beams," *Int. J. Impact Eng.*, vol. 93, pp. 153–165, 2016.